AD-A129 201 HEIGHT PROFILES OF TRANSPOLOR VLF/LF SIGNALS(U) 1/1
PACIFIC-SIERRA RESEARCH CORP LOS ANGELES CA E C FIELD
01 JAN 82 PSR-1128 DNA-5935F DNA001-79-C-0015
UNCLASSIFIED F/G 17/2.1 NL

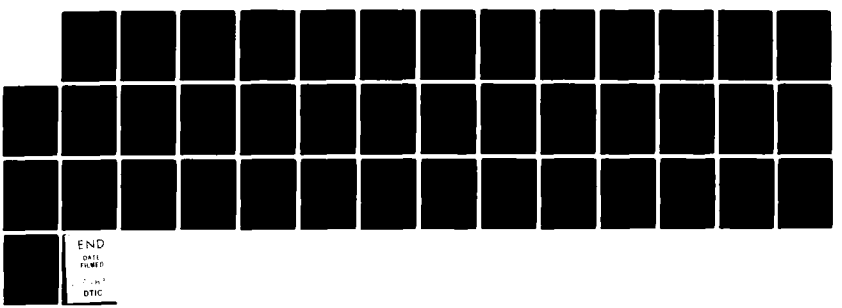

END
DATE FILMED
DTIC

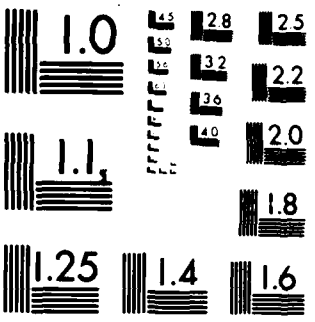

DNA 5935F

HEIGHT PROFILES OF TRANSPOLOR VLF/LF SIGNALS

E. C. Field, Jr.
Pacific-Sierra Research Corporation
12340 Santa Monica Boulevard
Los Angeles, California 90025

1 January 1982

Final Report for Period 1 December 1978—1 January 1982

CONTRACT No. DNA 001-79-C-0015

APPROVED FOR PUBLIC RELEASE;
DISTRIBUTION UNLIMITED.

THIS WORK WAS SPONSORED BY THE DEFENSE NUCLEAR AGENCY
UNDER RDT&E RMSS CODE B322079464 S99QAXHB04221 H2590D.

Prepared for
Director
DEFENSE NUCLEAR AGENCY
Washington, DC 20305

Destroy this report when it is no longer needed. Do not return to sender.

PLEASE NOTIFY THE DEFENSE NUCLEAR AGENCY, ATTN: STTI, WASHINGTON, D.C. 20305, IF YOUR ADDRESS IS INCORRECT, IF YOU WISH TO BE DELETED FROM THE DISTRIBUTION LIST, OR IF THE ADDRESSEE IS NO LONGER EMPLOYED BY YOUR ORGANIZATION.

UNCLASSIFIED

SECURITY CLASSIFICATION OF THIS PAGE (When Data Entered)

REPORT DOCUMENTATION PAGE	READ INSTRUCTIONS BEFORE COMPLETING FORM
1. REPORT NUMBER: DNA 5935F	2. GOVT ACCESSION NO.: AD-A129 201
3. RECIPIENT'S CATALOG NUMBER:	
4. TITLE (and Subtitle): HEIGHT PROFILES OF TRANSPOLAR VLF/LF SIGNALS	5. TYPE OF REPORT & PERIOD COVERED: Final Report for Period 1 Dec 78 - 1 Jan 82
	6. PERFORMING ORG. REPORT NUMBER: PSR Report 1128
7. AUTHOR(s): E. C. Field, Jr.	8. CONTRACT OR GRANT NUMBER(s): DNA 001-79-C-0015
9. PERFORMING ORGANIZATION NAME AND ADDRESS: Pacific-Sierra Research Corporation, 12340 Santa Monica Boulevard, Los Angeles, California 90025	10. PROGRAM ELEMENT, PROJECT, TASK AREA & WORK UNIT NUMBERS: Subtask S99QAXHB042-21
11. CONTROLLING OFFICE NAME AND ADDRESS: Director, Defense Nuclear Agency, Washington, D.C. 20305	12. REPORT DATE: 1 January 1982
	13. NUMBER OF PAGES: 40
14. MONITORING AGENCY NAME & ADDRESS(if different from Controlling Office)	15. SECURITY CLASS. (of this report): UNCLASSIFIED
	15a. DECLASSIFICATION/DOWNGRADING SCHEDULE: N/A since UNCLASSIFIED

16. DISTRIBUTION STATEMENT (of this Report)

Approved for public release; distribution unlimited.

17. DISTRIBUTION STATEMENT (of the abstract entered in Block 20, if different from Report)

18. SUPPLEMENTARY NOTES

This work was sponsored by the Defense Nuclear Agency under RDT&E RMSS Code B322079464 S99QAXHB04221 H2590D.

19. KEY WORDS (Continue on reverse side if necessary and identify by block number)

VLF/LF propagation
VLF/LF communication

20. ABSTRACT (Continue on reverse side if necessary and identify by block number)

Airborne trailing-wire antennas assume a nearly horizontal orientation during high-speed operations, causing most of the radiated energy to propagate in the transverse-electric (TE) mode. Such TE signals can be exploited for very-low-frequency (VLF) and low-frequency (LF) air-to-air communications.

The Defense Nuclear Agency and the Rome Air Development Center plan to measure the excitation and transpolar propagation of VLF/LF TE signals under normal ionospheric conditions and during solar proton events (SPEs), which

DD FORM 1 JAN 73 1473 EDITION OF 1 NOV 65 IS OBSOLETE

UNCLASSIFIED

SECURITY CLASSIFICATION OF THIS PAGE (When Data Entered)

20. ABSTRACT (cont.)

simulate aspects of certain nuclear environments. Measurements will also be made of transverse magnetic (TM) signals, in order to compare their behavior with that of the TE signals. The measurements will be made at altitudes between the ground and lower ionosphere with rocket-borne receivers, launched from Thule, Greenland.

This report presents calculated TE and TM signals at Thule for the ground-based and airborne transmitters to be monitored. The results can be used to specify the required receiver sensitivity and to predict transpolar TE/TM link performance under diverse ionospheric conditions.

SUMMARY

Airborne trailing-wire antennas assume a nearly horizontal orientation during high-speed operations, causing most of the radiated energy to propagate in the transverse-electric (TE) mode. Such TE signals can be exploited for very-low-frequency (VLF) and low-frequency (LF) air-to-air communications.

The Defense Nuclear Agency and the Rome Air Development Center plan to measure the excitation and transpolar propagation of VLF/LF TE signals under normal ionospheric conditions and during solar proton events (SPEs), which simulate aspects of certain nuclear environments. Measurements will also be made of transverse magnetic (TM) signals, in order to compare their behavior with that of the TE signals. The measurements will be made at altitudes between the ground and lower ionosphere with rocket-borne receivers, launched from Thule, Greenland.

This report presents calculated TE and TM signals at Thule for the ground-based and airborne transmitters to be monitored. The results can be used to specify the required receiver sensitivity and to predict transpolar TE/TM link performance under diverse ionospheric conditions.

PREFACE

This report provides theoretical inputs to a forthcoming experiment, supported in part by the Defense Nuclear Agency, that will measure the strengths and height profiles of horizontally polarized VLF/LF signals at Thule, Greenland. It calculates height profiles of transverse electric (TE) and transverse magnetic (TM) signals from several ground-based and airborne transmitters during normal daytime and a strong solar proton event. The latter simulates aspects of a nuclear environment. The analysis and results are useful for predicting transpolar TE/TM link performance under diverse ionospheric conditions.

TABLE OF CONTENTS

LIST OF ILLUSTRATIONS

SECTION 1

INTRODUCTION

Airborne trailing-wire antennas assume a nearly horizontal orientation during high-speed operations, causing most of the radiated energy to be horizontally polarized. Because of the nearly horizontal polarization, transverse electric (TE) signals can be exploited for very-low-frequency (VLF) and low-frequency (LF) air-to-air communications. Nonetheless, for many years military aircraft have used transverse magnetic (TM) antennas. Only recently has the installation of TE receivers begun.

Since TM signals have been used operationally, whereas TE signals have not, the measurement and analysis of TE signals have been less comprehensive than that of TM signals. Accordingly, the Defense Nuclear Agency (DNA) and Rome Air Development Center (RADC) plan to measure the excitation and transpolar propagation of VLF/LF signals under normal and disturbed ionospheric conditions. The present report provides theoretical support for that experiment by calculating height profiles of the signals to be measured.

Previous research [Lewis and Harrison, 1975; Kossey et al., 1981; Pappert, 1970; Field, 1975; Field et al., 1976; Field, 1981a, 1981b] suggests that, for air-to-air links, TE signals offer both advantages and disadvantages relative to TM signals. The advantages are as follows:

- Efficient excitation by nearly horizontal towed antennas.
- No degradation by poorly conducting ground, such as exists throughout Greenland and much of Canada.
- Protection against ground-based jammers.
- Low atmospheric noise.
- Filling of TM interference nulls.

The disadvantages include

- Greater vulnerability than TM signals to degradation during ionospheric disturbances (except for propagation over poorly conducting ground).
- Slightly poorer propagation than TM signals under normal conditions.
- A null in the end-fire transmission direction.

The forthcoming experiment will use rocket-borne receivers to measure TE and TM signals across the entire width of the earth-ionosphere waveguide; that is, measurements will be made at all altitudes between the ground and the lower ionosphere. The rockets will be launched from Thule, Greenland, and the payload will monitor several transmitters that are located in and near the continental United States (CONUS). The plan includes vertically polarized ground-based transmitters and horizontally polarized airborne transmitters, although arrangements for the latter are not yet final. Measurements will be made under normal conditions and, it is hoped, during solar proton events (SPEs).

If the experiment is fully successful, it will obtain previously unavailable data on

- The effect of a strong ionospheric disturbance on TE signals.*
- TE propagation across poorly conducting regions of Canada.*
- The ability of a ground-based transmitter to exploit geomagnetic conversion as a means of creating a horizontally polarized signal at elevated receivers.

Those data will be relevant to certain of the above-listed advantages and disadvantages of TE signals, namely, their predicted superior

*The transpolar TM signal has already been measured [Oelberman et al., 1969; Westerlund et al., 1969; Field et al., 1972; Westerlund and Reder, 1973].

propagation over poorly conducting ground, effectiveness against ground-based jammers, and vulnerability to ionospheric disturbances--such as occurs in a nuclear environment.

This report presents theoretical predictions of the TE and TM signals at Thule for several of the transmitters to be monitored. The results can be used to specify the required receiver sensitivity and bandwidth, as well as to predict transpolar TE/TM link performance under diverse ionospheric conditions.

SECTION 2

DESCRIPTION OF EXPERIMENT

This section summarizes the planned transpolar propagation experiment. Some aspects of the plan are tentative and thus subject to revision. The greatest uncertainty is the availability of the airborne terminals, described below.

EXPERIMENTAL OBJECTIVE

The experiment is designed to obtain much-needed data on the performance of air-to-air VLF/LF TE signals under the following three stressed conditions: (1) strong ionospheric disturbance, (2) low ground conductivity on the propagation path, and (3) presence of a vertically polarized ground-based jammer.

The data will be measured with elevated TE and TM receivers, which will monitor a number of ground-based and airborne transmitters. The receivers will be in the polar cap, and the propagation paths will traverse poorly conducting regions in Canada. If possible, the measurements will be coordinated with one or more strong SPEs, which cause ionospheric disturbances resembling a nuclear environment.

RECEIVERS

The receivers will be carried by rockets to altitudes of at least 70 km. The orientation of the package is nearly vertical, so orthogonal loops will sense the TE (horizontal loop) and TM (vertical loop) components of a signal. The data will be transmitted to ground on a telemetry link. That configuration, which has been used successfully [Harrison et al., 1981], will therefore give height profiles of TE and TM fields between the ground and the lower ionosphere.

The receivers will be launched from Thule, Greenland, which is well within the polar cap. Auxiliary measurements will be made with VLF sounders at Thule to determine the occurrence and structure of

SPE-induced ionospheric disturbances. Satellite measurements of incident proton fluxes and spectrums will be used, if available.

TRANSMITTERS

Many VLF/LF transmitters might produce a detectable signal at Thule. By monitoring all such transmitters, the TE and TM signals can be measured simultaneously, thus permitting their behavior to be compared. The transmitters and propagation paths treated in the present report are shown in Fig. 1, and their characteristics are summarized in Table 1.

Table 1. Transmitter characteristics.

Transmitter	Elevation	Polarization	Nominal Power (kw)	Nominal Frequency (kHz)
NAA	Ground-based	Vertical	1000	18
NLK	Ground-based	Vertical	1000	18
Silver Creek	Ground-based	Vertical	50	35
Hawes	Ground-based	Vertical	50	35
TACAMO	~20,000 ft	~90% horizontal	200	20
CINCLANT ABNCP	~30,000 ft	~90% horizontal	10	35

All of the ground-based transmitters are vertically polarized. The airborne transmitters will be flown at high speed, causing their antennas to be inclined about 15 deg with respect to the horizontal. The exact locations of the airborne transmitters cannot be predicted, so a nominal location is shown.

Figure 1 also shows estimated ground conductivities along the propagation paths [Westinghouse Electric Corporation, 1968]. We emphasize that many of the estimates were inferred from geological structure rather than actual conductivity measurements. They are therefore subject to considerable uncertainty. Nonetheless, the map shows that all paths traverse regions having very low conductivity.

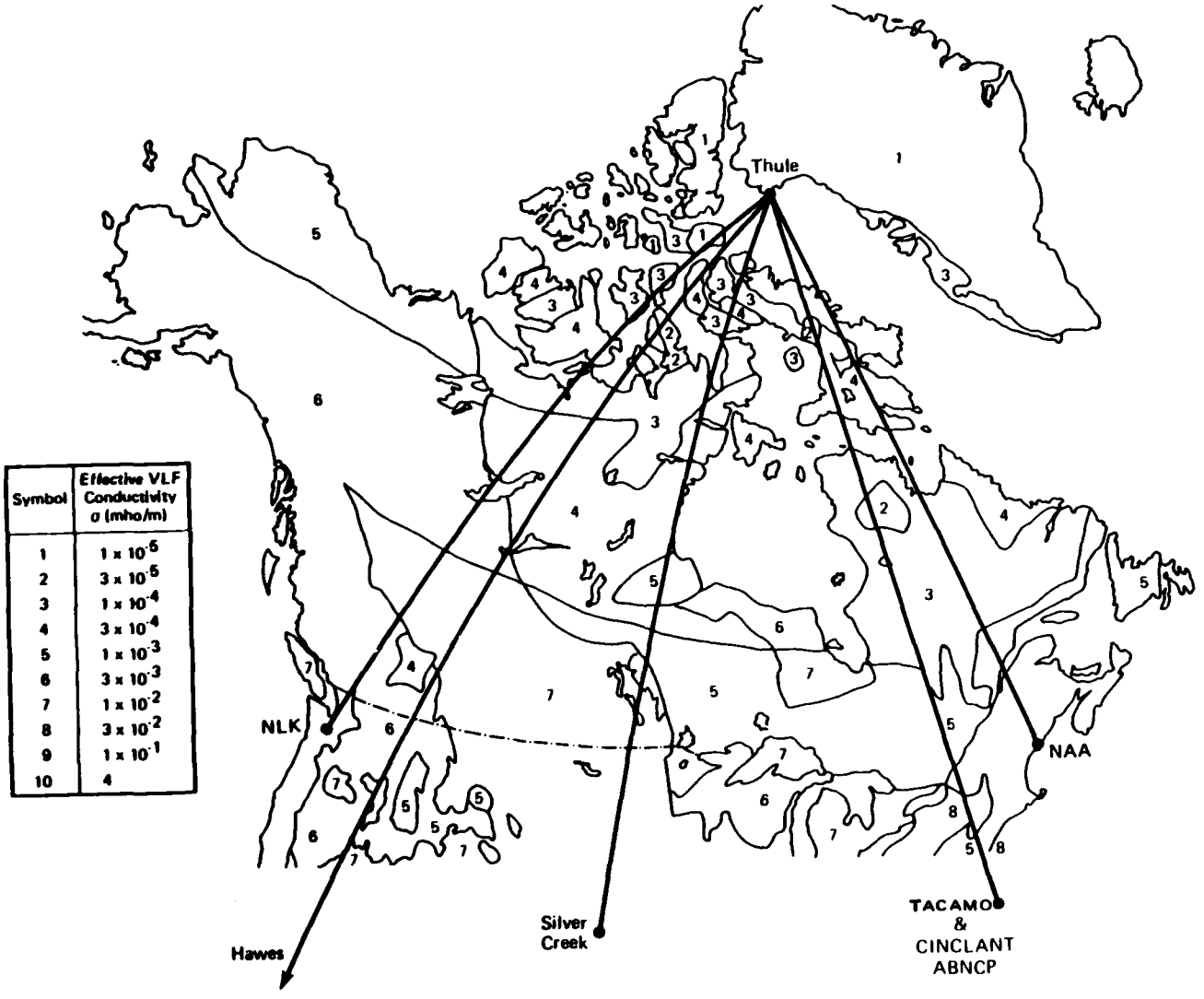

Symbol	Effective VLF Conductivity σ (mho/m)
1	1×10^{-5}
2	3×10^{-5}
3	1×10^{-4}
4	3×10^{-4}
5	1×10^{-3}
6	3×10^{-3}
7	1×10^{-2}
8	3×10^{-2}
9	1×10^{-1}
10	4

Figure 1. Map of transpolar VLF/LF propagation experiment.

OCCURRENCE OF SPEs

In order to simulate nuclear environments that severely constrict the earth-ionosphere waveguide, an SPE must contain a substantial flux of energetic protons. Figure 2 superimposes the time frame of the current solar cycle on the occurrence of such SPEs during the previous two cycles. If history repeats itself--by no means certain--the strongest SPEs will occur in 1982 and 1983, somewhat beyond the peak in the cycle.

SPEs persist for several days, with the strongest effects occurring in the first day or so. As a result, rocket launches and transmissions must be coordinated on about 24 hours' notice. Such coordination appears feasible, although final arrangements have yet to be made for the airborne transmitters.

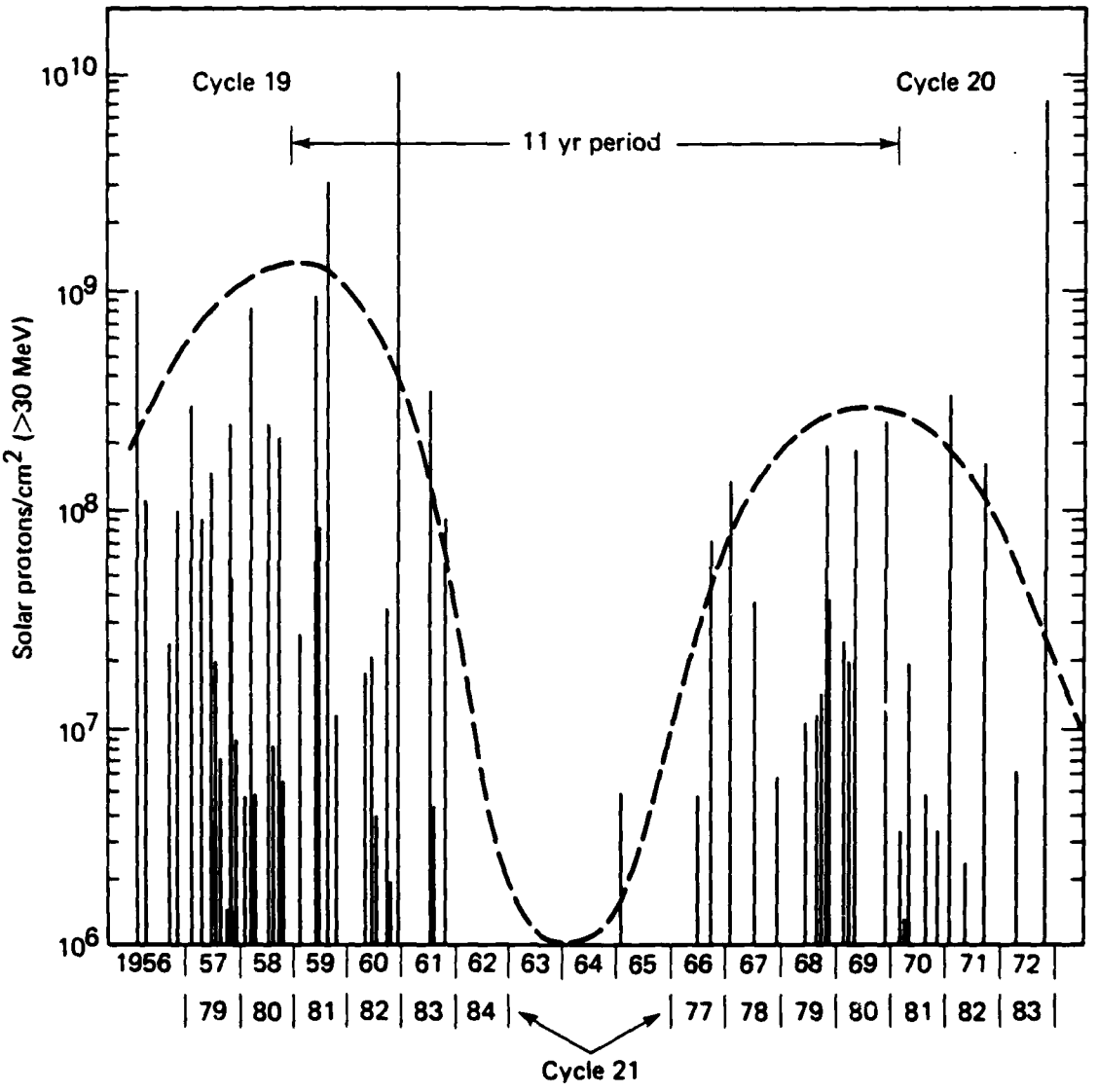

Figure 2. Occurrence of SPEs with protons having energy greater than 30 MeV (Lockheed Missiles and Space Company, 1977).

SECTION 3

PROPAGATION EQUATIONS

The detailed equations governing VLF propagation have appeared elsewhere (e.g., Galejs [1972], Wait [1970], Field et al. [1976]), so need not be repeated here. We solve them numerically, using the method of Field et al. [1976], accounting for the vertical inhomogeneity of the ionosphere and curvature of the earth. To define the notation and illustrate the key dependences, we recapitulate the equations that govern the electric field when geomagnetic anisotropy can be neglected. That approximation is very accurate when the upper boundary of the earth-ionosphere waveguide is depressed far below its normal level; and it is fairly accurate for long-range propagation under normal daytime conditions.

The TM and TE waveguide modes do not exist independently when geomagnetic anisotropy is important. Instead, they are coupled, with the TM mode having a horizontally polarized component and the TE mode a vertically polarized component. Under such conditions, vertical and horizontal electric dipole antennas will excite *both* TM and TE waveguide modes. That geomagnetic coupling is most pronounced when significant amounts of energy penetrate to--and are reflected from--altitudes above about 75 km, where the gyrofrequency exceeds the collision frequency. Such high reflection altitudes can occur (1) on short paths where the waves are steeply incident on the ionosphere, or (2) during normal nighttime, when the ionospheric D-layer is rarefied. This report concentrates on propagation under normal daytime and disturbed conditions where geomagnetic coupling is small or negligible.

TRANSVERSE MAGNETIC MODES

Typically, VLF/LF transmitters are vertically oriented, and their fields are composed of a superposition of TM modes. The vertical electric field is given by

$$E_V = -120\pi i\, e^{-\pi i/4}\, \frac{IL \cos\psi}{\sqrt{\lambda d}} \sqrt{\frac{d/a}{\sin d/a}} \sum_{\ell} S_\ell^{3/2}\, \Lambda_\ell \exp\left(-\frac{\beta_\ell d}{8.7}\right)$$

$$\times \exp\left(-\frac{2\pi i}{\lambda}\frac{c}{v_\ell} d\right) G_\ell(h_T) G_\ell(h_R) \quad V/m\ , \qquad (1)$$

where the subscript ℓ denotes quantities associated with the ℓth TM mode, IL is the effective electric dipole moment of the transmitting antenna, λ is the free-space wavelength, d is the distance from the transmitter, a is the earth's radius, and c is the speed of light. We have included a factor cos ψ--where ψ is the angle between the dipole orientation and the vertical--to account for inclined transmitting antennas. Of course, cos $\psi = 1$ for a vertical electric dipole. Although most quantities are in MKS units, we express all distances (L, λ, d, a) in megameters.

The quantity S_ℓ is the eigenvalue of the ℓth TM mode. At VLF, however, S has a magnitude close to unity, so the term $S_\ell^{3/2}$ in Eq. (1) does not appreciably influence the field. The magnitude of the vertical electric field depends on the state of the ionosphere through three parameters: Λ_ℓ, the excitation factor for the TM mode; β_ℓ, the attenuation rate in decibels per megameter of propagation (dB/Mm); and G_ℓ, the height-gain function for transmitter and receiver heights h_T and h_R, respectively. The phase of the ℓth mode is governed by the relative phase velocity v_ℓ/c. These propagation parameters must all be computed numerically for model ionospheres having arbitrary height profiles.

TRANSVERSE ELECTRIC MODES

Airborne VLF/LF transmitters use trailing-wire antennas whose primary orientation is often horizontal. Such antennas radiate a complicated superposition of TM and TE modes. Here we avoid much of that complexity by considering broadside propagation, where the great-circle path connecting transmitter and receiver is perpendicular to the plane containing the inclined electric-dipole transmitting antenna.

The vertical electric field produced by the vertical component of the inclined transmitting antenna is given by Eq. (1). The broadside horizontal electric field produced by the horizontal component is given by

$$E_H = -120\pi i\, e^{-\pi i/4}\, \frac{IL \sin\psi}{\sqrt{\lambda d}} \sqrt{\frac{d/a}{\sin d/a}} \sum_m S_m^{-1/2}\, \Lambda_m \exp\left(-\frac{\beta_m d}{8.7}\right)$$

$$\times \exp\left(-\frac{2\pi i}{\lambda}\frac{c}{v_m} d\right) G_m(h_T) G_m(h_R) \quad \text{V/m} . \tag{2}$$

The symbols are the same as in Eq. (1), except that m denotes the *mth* TE mode.

SINGLE-MODE APPROXIMATION

High-order modes are more heavily attenuated than low-order ones. A major simplification therefore occurs for long propagation paths, where only the first TM ($\ell = 1$) or TE ($m = 1$) mode is important. The summations in Eqs. (1) and (2) are then not needed and, after some rearrangement, the field magnitudes can be written

$$|E_V| \approx 9.5 P^{1/2} \cos\psi \left(\frac{\lambda}{d}\right)^{1/2} \Lambda_V G_V(h_T) G_V(h_R) \exp\left(-\frac{\beta_V d}{8.7}\right) \quad \text{V/m} , \tag{3}$$

$$|E_H| \approx 14 P^{1/2} \sin\psi \left(\frac{\lambda}{d}\right)^{1/2} \Lambda_H G_H(h_T) G_H(h_R) \exp\left(-\frac{\beta_H d}{8.7}\right) \quad \text{V/m} . \tag{4}$$

To derive Eqs. (3) and (4) from Eqs. (1) and (2), we have assumed d/a to be small, $S \approx 1$, and used subscripts V and H to denote $\ell = 1$ and $m = 1$, respectively. P denotes the radiated power. The constant factors in Eqs. (3) and (4) differ because we assumed a short antenna in Eq. (3), but a resonant half-wave antenna in Eq. (4). Our assumption

of an idealized resonant horizontal antenna somewhat overestimates the horizontal fields.

Equations (3) and (4) pertain to uniform propagation paths. However, the paths shown in Fig. 1 are nonuniform because of the polar cap boundary and lateral variations of ground conductivity. Those equations can be generalized to approximately describe nonuniform paths by substituting

$$\Lambda G(h_T)G(h_R) \rightarrow \left[\Lambda_T^{1/2}(\sigma_T)G(\sigma_T,\ h_T)\right]\left[\Lambda_R^{1/2}(\sigma_R)G(\sigma_R,\ h_R)\right] \qquad (5)$$

and

$$\exp\left(-\frac{\beta d}{8.7}\right) \rightarrow \exp\left(-\sum_i \frac{\beta_i\ \Delta d_i}{8.7}\right)\ , \qquad (6)$$

where σ denotes ground conductivity, and β_i and Δd_i are, respectively, the attenuation rate and length of the *ith* path segment. Although Eqs. (3) through (6) are much simpler than Eqs. (1) and (2), we must still compute Λ, G, and β numerically.

SECTION 4

CALCULATED SIGNAL HEIGHT PROFILES

This section computes field-strength height profiles at Thule during normal daytime and a strong SPE. The results for normal daytime are based on the DNA model ambient ionosphere, as reported, for example, by Pappert and Moler [1974]. It is impossible to accurately predict the fields during a forthcoming SPE, because no two SPEs are identical. We therefore use a model for a nominal disturbed ionosphere that applies equally well to a strong SPE or a moderate nuclear environment. This model and others have been published several times (e.g., Field [1981a, 1981b], Field et al. [1976]) and, for brevity, will not be repeated here.

TEST OF SINGLE-MODE APPROXIMATION

Figure 3 compares E_H calculated for normal daytime from Eq. (2) using five modes with that from Eq. (4) using only the m = 1 mode. The assumed transmitter height of 9 km, power of 10 kW, and frequency of 35 kHz represent the CINCLANT ABNCP (see Table, p. 9). The assumed receiver height of 25 km corresponds to about one-third of the maximum altitude of the payload. Those parameters constitute a stringent test of the single-mode approximation because they emphasize high-order modes, which are less important for lower frequencies or TM signals.

The multimode field shows pronounced maxima and minima out to distances of 4 or 5 Mm, whereas the single-mode result falls off smoothly with distance. We conclude that during normal daytime the single-mode approximation is marginally accurate at a distance of 4 Mm and very accurate beyond 5 Mm.

Figure 4 compares the multimode and single mode calculations for propagation during a strong SPE. All other input parameters are the same as for Fig. 3. The mode structure is much less pronounced than for normal daytime propagation because the higher modes are

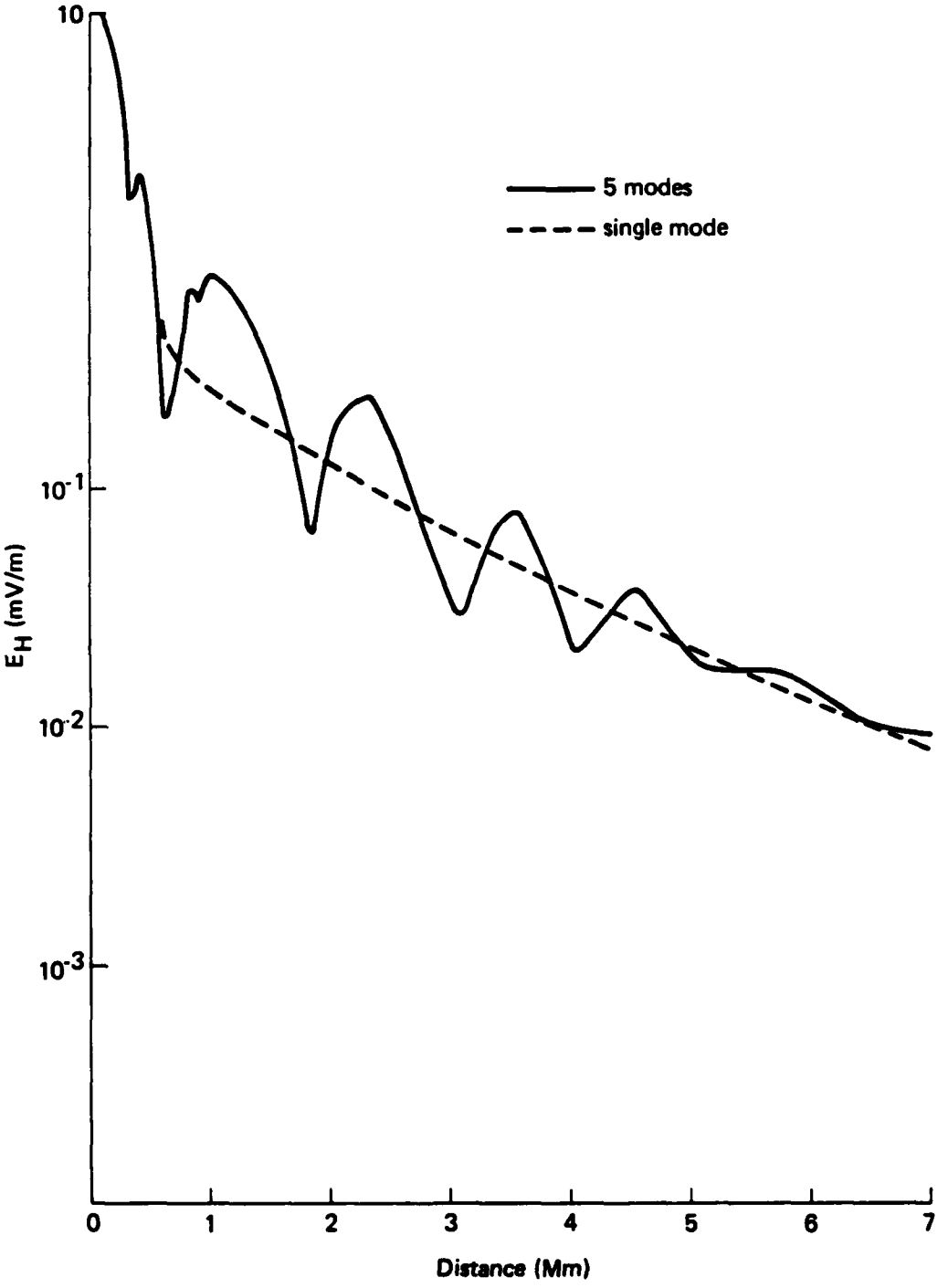

Figure 3. Comparison of multimode and single-mode calculations of TE signal during normal daytime: h_T = 9 km, h_R = 25 km, f = 35 kHz, P = 10 kW.

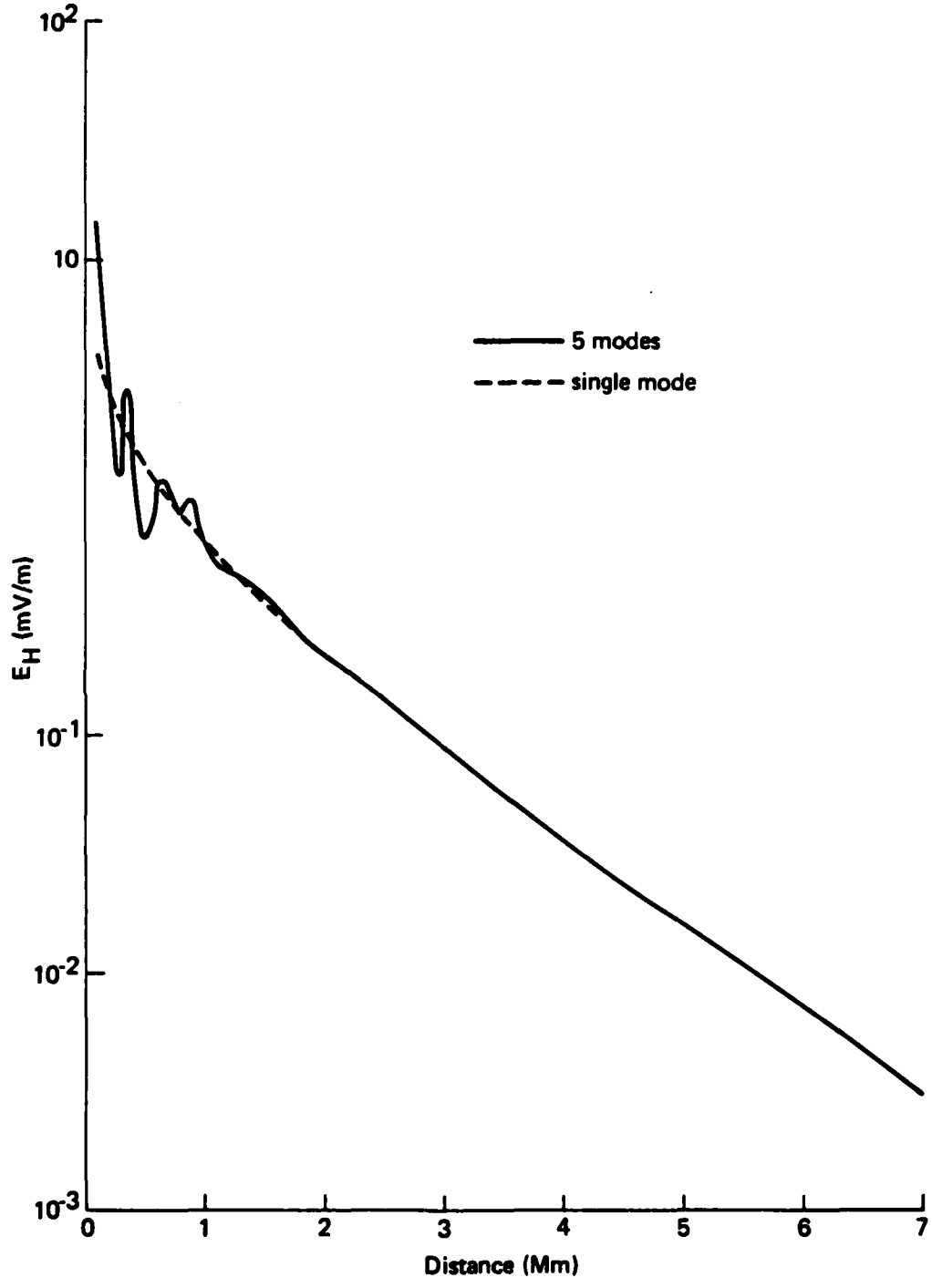

Figure 4. Comparison of multimode and single-mode calculations of TE signal during a strong SPE: h_T = 9 km, h_R = 25 km, f = 35 kHz, P = 10 kW.

heavily attenuated by the disturbance. Consequently, the single-mode approximation is very accurate at distances beyond 1 Mm for propagation during a strong SPE.

UNCERTAINTIES IN GROUND CONDUCTIVITY

Figures 5 and 6 show the dependence on ground conductivity of the attenuation rates and excitation of the lowest TE and TM modes. Results at 20 kHz are given for normal daytime and a strong SPE. The disturbance increases the attenuation rate and excitation of both polarizations. The TE results are nearly independent of ground conductivity,* whereas the TM graphs exhibit broad maxima for conductivities between 3×10^{-5} and 3×10^{-4} mhos/m. The maxima occur where the eigenangle of the lowest TM mode approximates the Brewster's angle of the ground. TE modes have no Brewster's angle.

This extreme sensitivity of TM mode parameters to ground conductivity--combined with uncertain parameter values--causes great uncertainty in the calculation of transpolar TM signals. Much of Canada has ground conductivity in the range of greatest sensitivity (compare the curves in Fig. 5 with the map in Fig. 1), so a factor-of-two uncertainty in σ could cause β_V to be uncertain by several decibels per megameter--or even more during a strong SPE. No such uncertainty occurs in the calculation of air-to-air TE signals, because they are nearly independent of ground conductivity.

SEMIEMPIRICAL CALCULATION OF TM SIGNAL

As discussed above, uncertainty in the ground conductivity causes great uncertainty in the TM calculations. Fortunately, data are available for the normal daytime TM signal of several ground-based VLF transmitters that are routinely monitored at Thule with ground-based receivers [Kossey and Turtle, 1981]. We use the data

---

*This conclusion applies to the attenuation rate β_H and--if the terminals are sufficiently elevated--to the product $\Lambda_H G_H^2$. The individual factors Λ_H and G_H depend strongly on σ, as does the product $\Lambda_H G_H^2$ if the terminal altitudes are less than about 1.5 km [Field, 1981b].

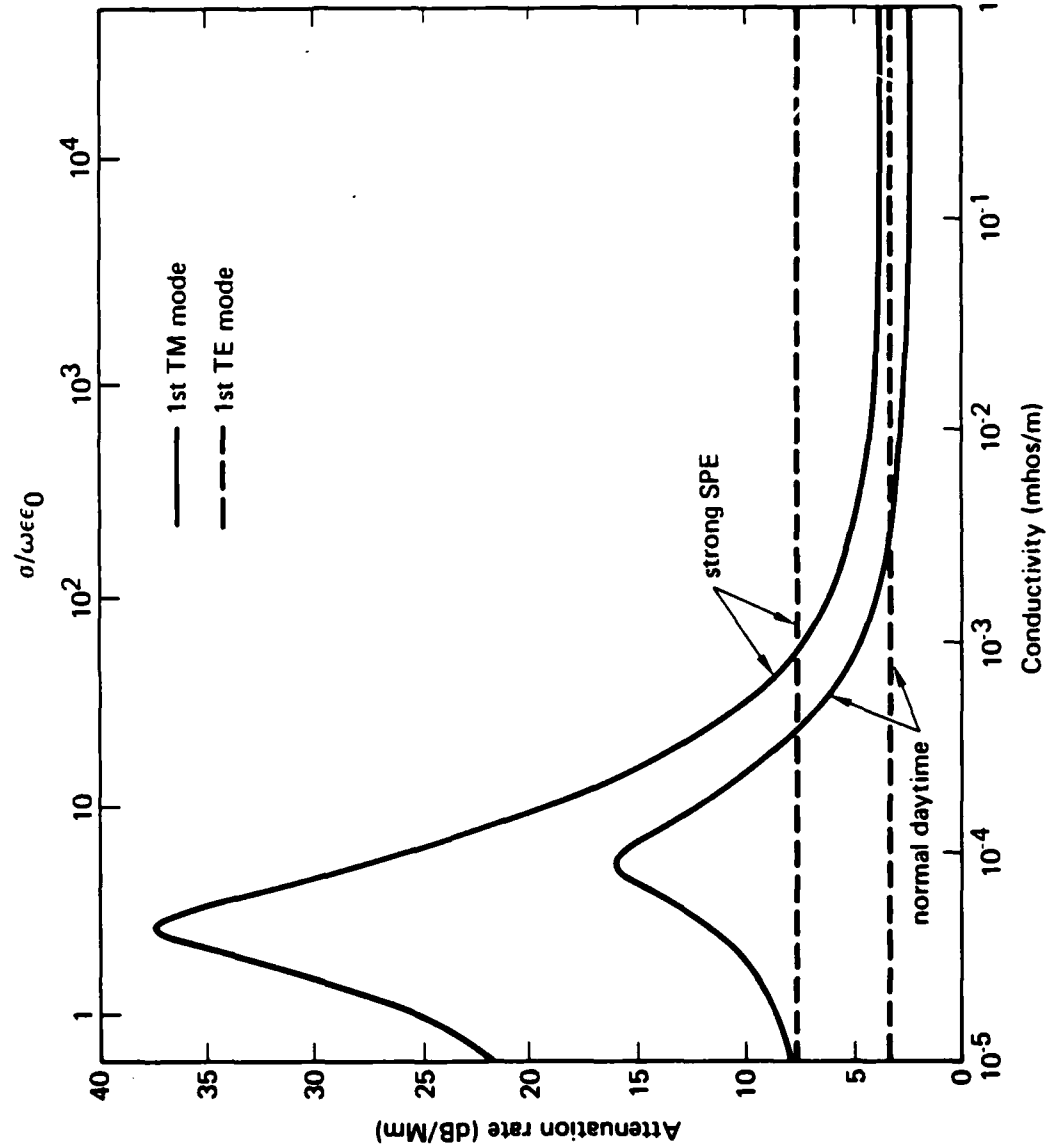

Figure 5. Attenuation rate β versus ground conductivity σ for normal daytime and strong SPE: f = 20 kHz.

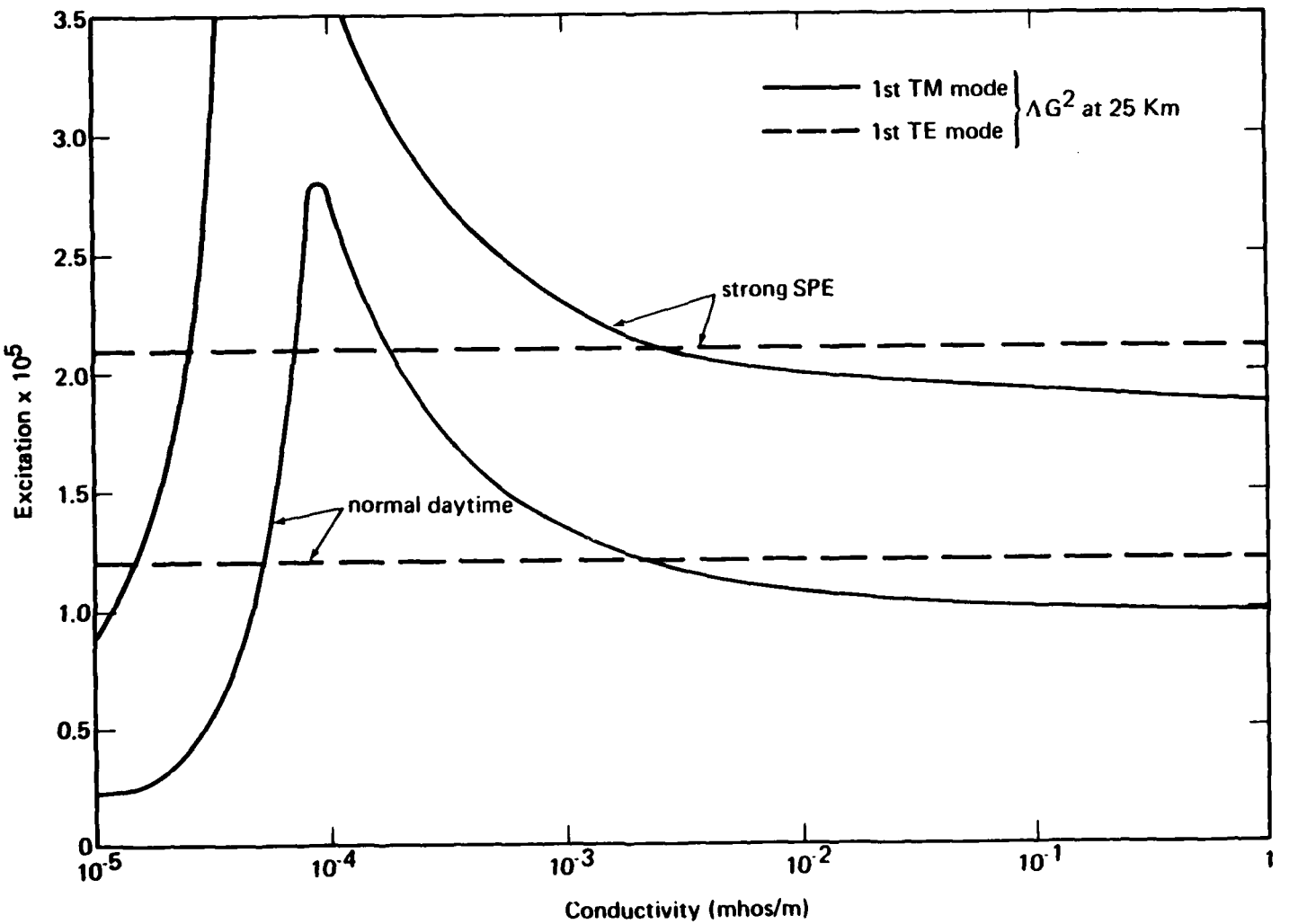

Figure 6. Excitation ΛG^2 versus ground conductivity σ for normal daytime and strong SPE: f = 20 kHz.

to normalize our calculated TM signals, thereby removing errors caused by poorly known values of ground conductivity.

Figure 7 plots the NAA-to-Thule TM signal as a function of distance, calculated from the single-mode approximation given by Eqs. (3), (5), and (6). The conductivity σ along the path, taken from Fig. 1, is shown at the top of Fig. 7. The abrupt changes in slope and magnitude of the graphs are caused, respectively, by the attenuation rate β_V and excitation factor A_V assuming different values in each conductivity segment.

Figure 7 reveals several unsatisfactory aspects of the ground-conductivity model. First, the calculated TM field depends strongly on the conductivity, which is poorly known. Second, the unrealistic abruptness of the field changes at the boundary of each conductivity segment results from the oversimplification of the model shown in Fig. 1; the true conductivity almost certainly does not exhibit the lateral discontinuities shown on the map. Finally, the field at Thule is ambiguous because Fig. 1 shows an abrupt change from sea-water (σ = 4 mhos/m) to ice ($\sigma = 10^{-5}$ mhos/m) at that location.*

Considering such problems, the calculated Thule signal of 0.35 to 0.5 mV/m is remarkably close to the average measured value of 0.18 mV/m. Nonetheless, since the measured value is certainly more accurate than the calculated one, we have normalized all NAA-to-Thule results to yield a ground-level field of 0.18 mV/m in normal daytime. That is, we have reduced all calculated NAA-to-Thule signals--normal and disturbed--by a factor of 2.4. We also use such normalization to calculate signals from other ground-based transmitters. Of course, the normalization factor differs for each transmitter.

Normalization to measured normal daytime signals is not possible for TE signals, because no data have been taken at Thule. However, our TE calculations should be more reliable than our TM calculations because they are unaffected by ground conductivity.

---

*The absence of a discontinuity at Thule for a strong SPE (Fig. 7) is a peculiarity of this specific ionosphere/ground model.

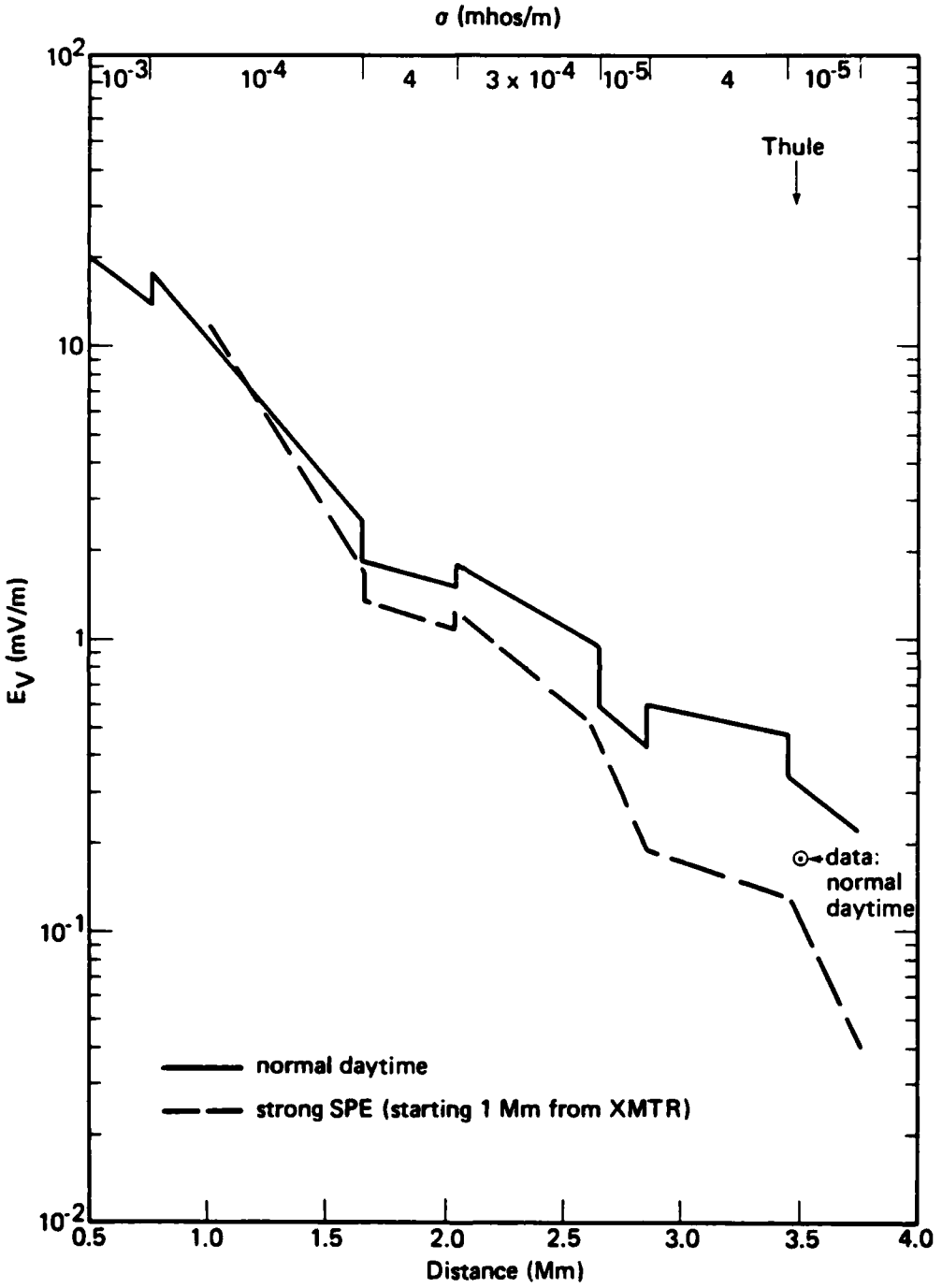

Figure 7. Single-mode calculation of NAA-to-Thule 18 kHz signal for normal daytime and strong SPE. Measured normal daytime signal at ground level is also shown.

CALCULATED FIELD HEIGHT PROFILES AT THULE

We next provide calculated height profiles of electric field strength at Thule for normal daytime and a strong SPE. The TM calculations are normalized to average measured daytime ground-level field strengths, as described above. The TE calculations are not normalized and correspond to broadside radiation from an ideal, resonant, half-wave antenna high above the ground. This idealization somewhat overestimates the signal strength. In all cases pertaining to the SPE, we assume the final 2500 Mm of the propagation path to be exposed to the disturbance; the initial segment of the path is during normal daytime. The calculated field-strength profiles, shown in Figs. 8 through 11, are largely self-explanatory.

Figure 8 pertains to the 18 kHz NAA-to-Thule path. We give profiles for assumed ground conductivities of 10^{-3} and 10^{-5} mhos/m because the true value at Thule is not evident from Fig. 1. The lower conductivity causes a whispering gallery effect such that the TM signal at altitudes of tens of kilometers is greater than the signal at the ground. The primary effects of the SPE on the unconverted signal are (1) to reduce the signal strength by about 10 dB and (2) to lower the effective top of the earth-ionosphere waveguide from about 65 km to about 45 km.

The geomagnetically converted signal profile shown in Fig. 8 is an empirical estimate based on (nonpolar) normal daytime data. A ground-based jammer would rely on such a signal to interfere with airborne reception of a TE signal. We emphasize that the estimate shown is crude, and that data on the converted signal are needed even for normal conditions. The converted signal would nearly vanish if a strong SPE or nuclear environment covered the entire propagation path, since it would be confined to altitudes too low to experience geomagnetic effects. However, no current theory can properly calculate the converted signal when conditions are mixed--i.e., normal daytime at the transmitter, but disturbances over the latter portion of the path. The planned experiment should obtain much-needed data on mixed-path phenomena.

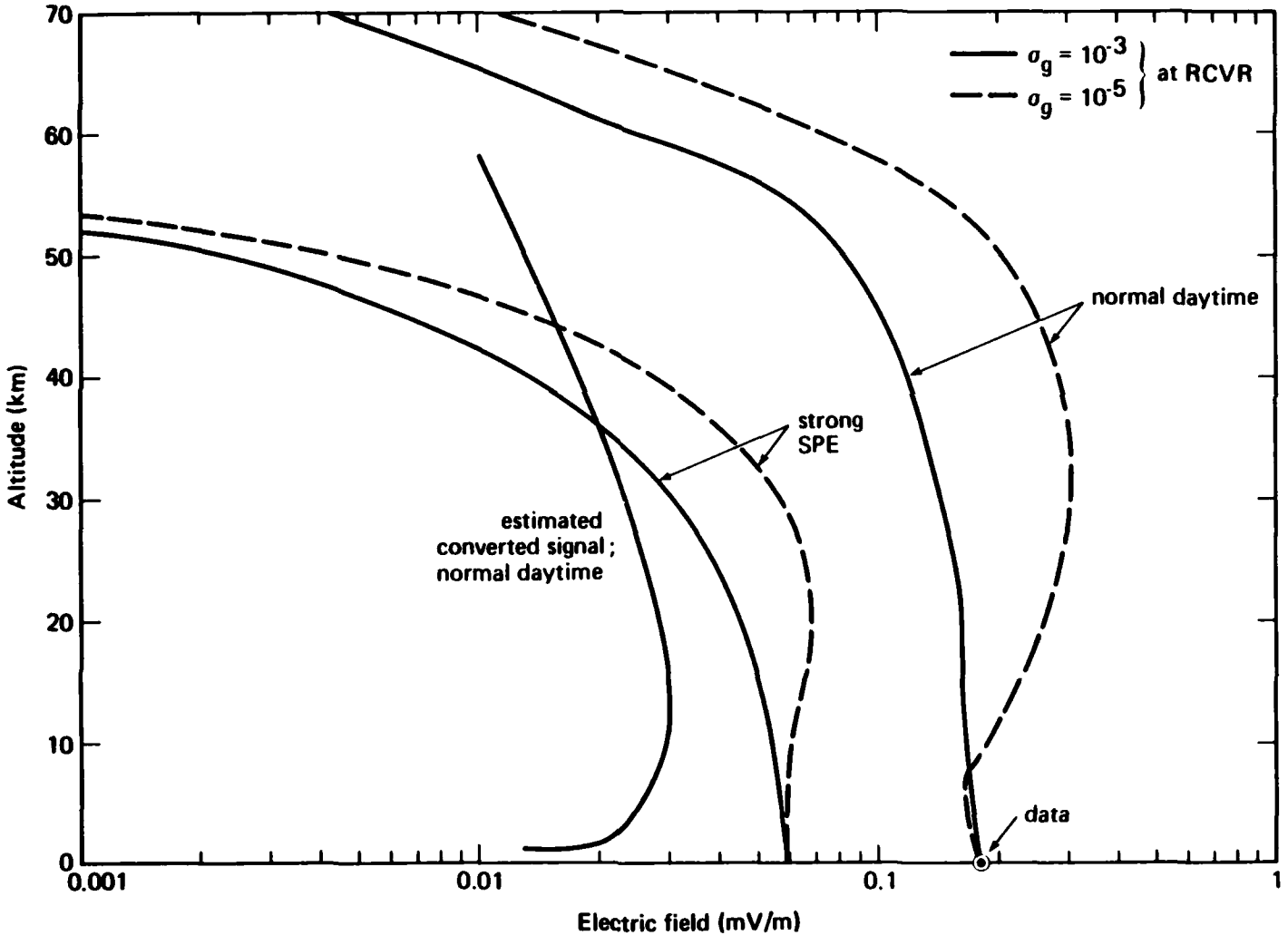

Figure 8. Calculated field height profiles for NAA-to-Thule signal.

Figure 9 pertains to the Silver Creek-to-Thule path. We use a nominal frequency of 35 kHz and radiated power of 50 kW. As expected, the signals are substantially weaker than those from the powerful NAA transmitter.

Figure 10 shows the broadside TE profile for a nominal TACAMO-to-Thule path. We assume TACAMO to be located as shown in Fig. 1, although another location might well occur. Also, we assume a 20 kHz frequency, a transmitter altitude of 20,000 ft, an antenna inclination angle of 75 deg (15 deg from horizontal), and--perhaps optimistically--a radiated power of 200 kW. The qualitative effects of the SPE on the TE signal are the same as on the TM signal--reduced strength and lowered waveguide height. The results calculated for $\sigma_R = 10^{-3}$ mhos/m are nearly identical with those for $\sigma_R = 10^{-5}$ mhos/m, confirming that air-to-air TE signals are nearly independent of ground conductivity.

Figure 11 presents similar profiles pertaining to the CINCLANT ABNCP at the location shown in Fig. 1. We assume nominal radiated power and frequency of 10 kW and 35 kHz, respectively, and a transmitter altitude of 30,000 ft. Because of the much lower radiated power, the CINCLANT ABNCP signal is much weaker and more difficult to detect than the TACAMO signal.

The Hawes-to-Thule signal is structurally identical to the Silver Creek-to-Thule signal shown in Fig. 10, but about 15 dB weaker. The NLK-to-Thule signal height profile is nearly the same as for the NAA-to-Thule signal shown in Fig. 9, but about 3 dB weaker.

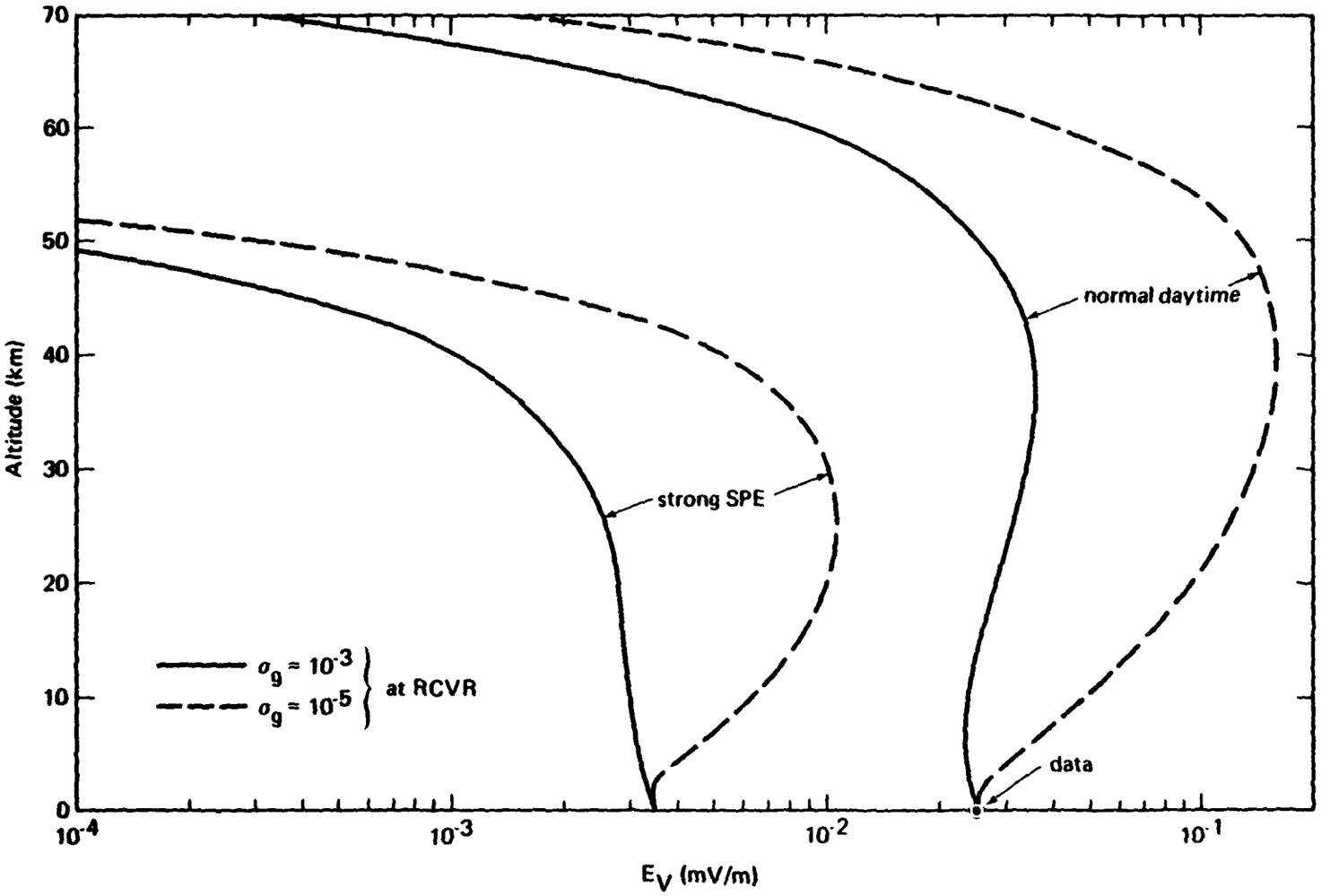

Figure 9. Calculated field height profiles for Silver Creek-to-Thule signal.

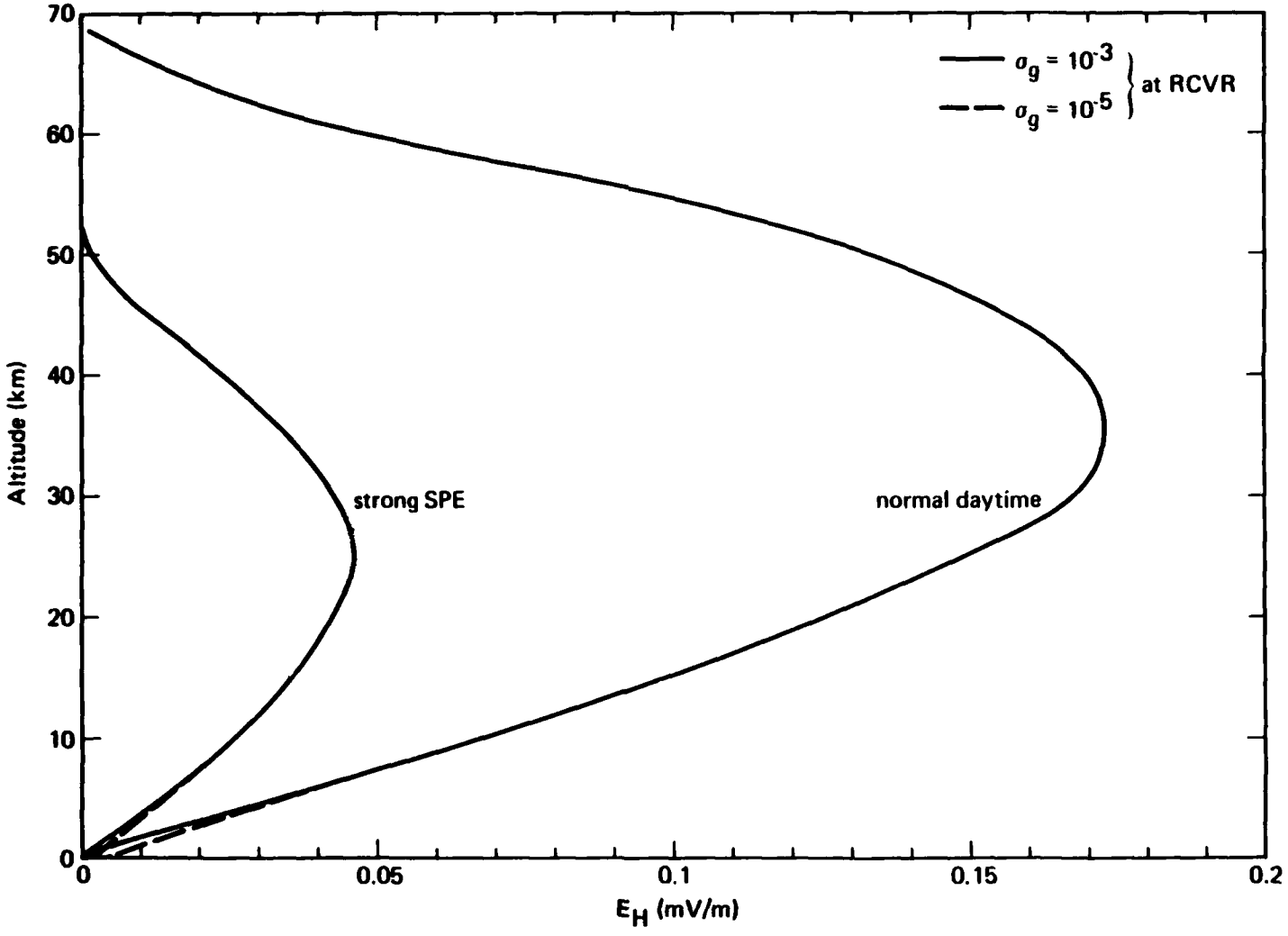

Figure 10. Calculated broadside TE field height profiles for TACAMO-to-Thule signal: f = 20 kHz, h_T = 20,000 ft.

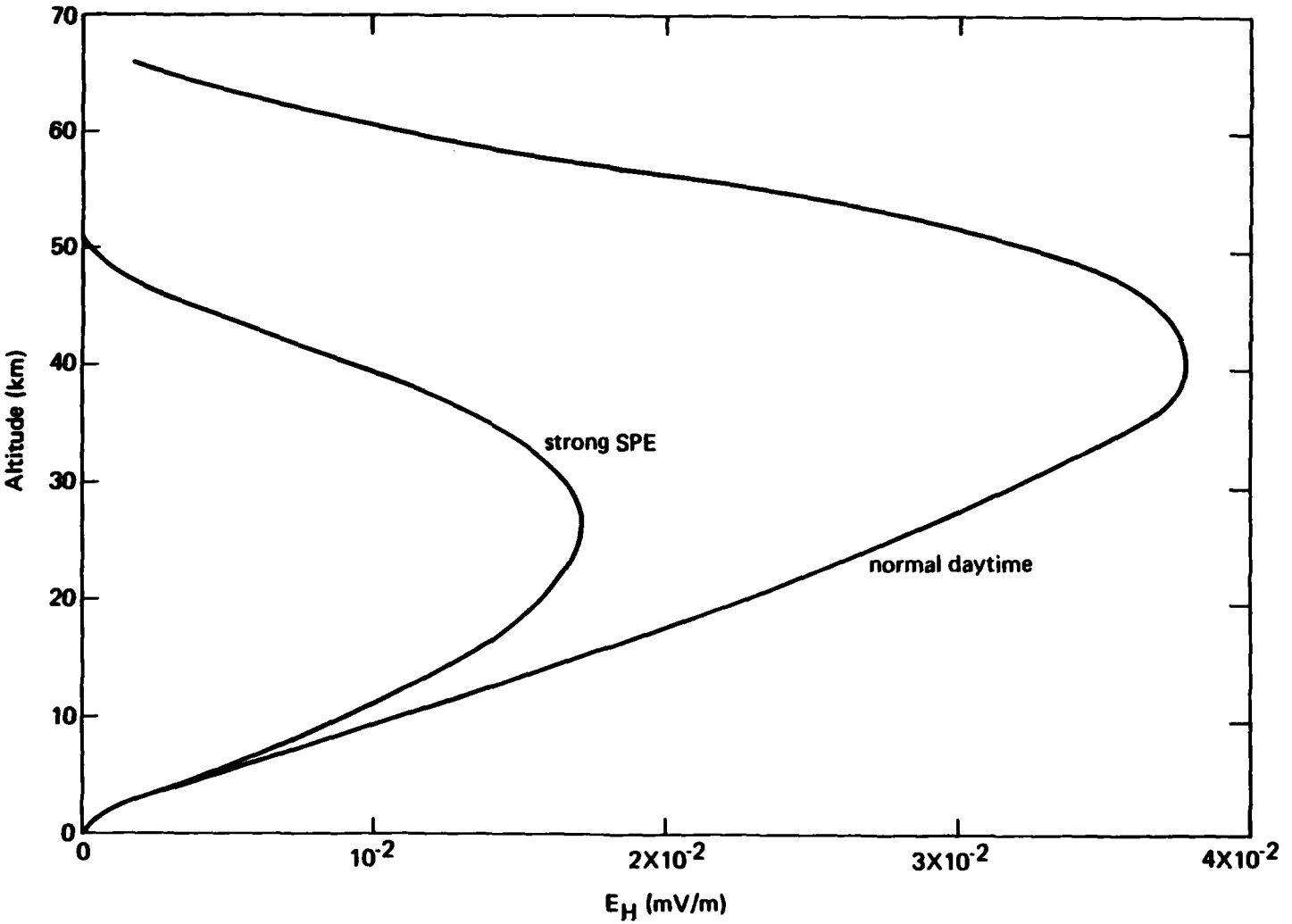

Figure 11. Calculated broadside TE field height profiles for CINCLANT ABNCP-to-Thule signal: f = 35 kHz, h_T = 30,000 ft.

REFERENCES

Field, E. C., *VLF/LF TE-Mode Propagation under Disturbed Ionospheric Conditions,* Air Force Cambridge Research Laboratory, AFCRL-TR-75-0382, July 1975.

Field, E. C., *Transverse Electric Waves for VLF/LF Communications Between Aircraft,* Pacific-Sierra Research Corporation, Report 1125, November 1981(a).

Field, E. C., "VLF in Disturbed Environments," presented at the Electromagnetic Wave Propagation Panel of NATO/AGARD, Brussels, Belgium, 21-25 September 1981(b) (available through the National Technical Information Service, Springfield, Virginia).

Field, E. C., et al., "Transpolar Propagation of Long Radio Waves," *J. Geophys. Res.*, Vol. 77, No. 7, March 1972, pp. 1264-1278.

Field, E. C., et al., *Effects of Antenna Elevation and Inclination on VLF/LF Signal Structure,* Air Force Systems Command, Rome Air Development Center, RADC-TR-76-C-375, December 1976.

Galejs, J., *Terrestrial Propagation of Long Electromagnetic Waves,* Pergamon Press, New York, 1972.

Harrison, R. P., et al., *TM/TE Polarization Ratios in a Sample of 30 kHz Sferics Received at Altitudes from 0 to 70 km,* Rome Air Development Center, RADC-TR-81-235, August 1981.

Kossey, P. A., and J. Turtle, Rome Air Development Center, Hanscom Air Force Base, Massachusetts, private communication, 1981.

Kossey, P. A., et al., "Relative Characteristics of TE/TM Waves Excited by Airborne VLF/LF Transmitters," presented at the Electromagnetic Wave Propagation Panel of NATO/AGARD, Brussels, Belgium, 21-25 September 1981 (available through the National Technical Information Service, Springfield, Virginia).

Lewis, E. A., and R. P. Harrison, *Experimental Evidence of a Strong TE-Polarized Wave from an Airborne LF Transmitter,* Air Force Cambridge Research Laboratory, AFCRL-TR-75-0555, October 1975.

Lockheed Missiles and Space Company, *Phase III Proposal for the Disturbed Media Satellite Program,* LMSC-D084927, October 1977.

Oelberman, E. J., et al., *Coordinated High-Latitude Experiments for the Simulation of Nuclear Burst Effects on VLF Systems,* HRB-Singer, State College, Pennsylvania, Report 336-F, February 1969.

Pappert, R. A., "Effects of Elevation and Ground Conductivity on Horizontal Dipole Excitation of the Earth-Ionosphere Waveguide," *Radio Sci.*, Vol. 5, March 1970, pp. 579-590.

Pappert, R. A., and W. F. Moler, "Propagation Theory and Calculations at Lower Extremely Low Frequencies (ELF)," *IEEE Trans. Comm.*, Vol. COM-22, April 1974, pp. 438-451.

Wait, J. R., *Electromagnetic Waves in Stratified Media*, Pergamon Press, New York, 1970.

Westerlund, S., and F. H. Reder, "VLF Radio Signals Propagating over the Greenland Ice-Sheet," *J. Atmos. Terr. Phys.*, Vol. 35, 1973, pp. 1475-1491.

Westerlund, S., et al., "Effects of Polar Cap Absorption Events on VLF Transmissions," *Planet. Space Sci.*, Vol. 17, 1969, pp. 1329-1374.

Westinghouse Electric Corporation, *World-Wide VLF Effective-Conductivity Map*, Report 80133F-1, January 1968.

DISTRIBUTION LIST

DEPARTMENT OF DEFENSE

Assistant to the Secretary of Defense
Atomic Energy
ATTN: Executive Assistant

Command & Control Technical Center
ATTN: C-650
ATTN: C-312, R. Mason
ATTN: C-650, G. Jones
3 cy ATTN: C-650, W. Heidig

Defense Communications Agency
ATTN: J300 for Yen-Sun Fu
ATTN: Code 230
ATTN: Code 205

Defense Communications Engr Center
ATTN: Code R410
ATTN: Code R410, N. Jones
ATTN: Code R123
ATTN: Code R410, R. Craighill

Defense Intelligence Agency
ATTN: DT-1B
ATTN: DB-4C, E. O'Farrell
ATTN: DB, A. Wise
ATTN: Dir
ATTN: DC-7B

Defense Nuclear Agency
ATTN: RAAE, P. Lunn
ATTN: NATD
ATTN: STNA
ATTN: RAEE
ATTN: NAFD
3 cy ATTN: RAAE
4 cy ATTN: TITL

Defense Technical Information Center
12 cy ATTN: DD

Dep Under Secretary of Defense
Comm, Cmd, Cont & Intell
ATTN: Dir of Intell Sys

Field Command
DNA/Det 1
Lawrence Livermore Lab
ATTN: FC-1

Field Command
Defense Nuclear Agency
ATTN: FCTT, G. Ganong
ATTN: FCTT, W. Summa
ATTN: FCPR

Interservice Nuclear Weapons School
ATTN: TTV

Joint Chiefs of Staff
ATTN: C3S Evaluation Office, HDOO
ATTN: C3S

Joint Strat Tgt Planning Staff
ATTN: JLTW-2
ATTN: JLA, Threat Applications Div

DEPARTMENT OF DEFENSE (Continued)

National Security Agency
ATTN: W-32, O. Bartlett
ATTN: R-52, J. Skillman
ATTN: B-3, F. Leonard

Under Secretary of Def for Rsch & Engrg
ATTN: Strat & Space Sys, OS
ATTN: Strat & Thtr Nuc Forces, B. Stephan

WWMCCS System Engineering Org
ATTN: J. Hoff

DEPARTMENT OF THE ARMY

Assistant Ch of Staff for Automation & Comm
ATTN: DAMO-C4, P. Kenny

Atmospheric Sciences Lab
US Army Electronics R&D Cmd
ATTN: DELAS-EO, F. Niles

BMD Advanced Technology Center
ATTN: ATC-T, M. Capps
ATTN: ATC-O, W. Davies
ATTN: ATC-R, W. Dickinson
ATTN: ATC-R, D. Russ

BMD Systems Command
ATTN: BMDSC-HLE, R. Webb
2 cy ATTN: BMDSC-HW

Dep Ch of Staff for Ops & Plans
ATTN: DAMO-RQC, C2 Div

Harry Diamond Labs
ATTN: DELHD-NW-R, R. Williams, 22000
2 cy ATTN: DELHD-NW-P, 20240

US Army Chemical School
ATTN: ATZN-CM-CS

US Army Comm-Elec Engrg Instal Agency
ATTN: CCC-CED-CCO, W. Neuendorf
ATTN: CCC-EMEO-PED, G. Lane

US Army Comm Command
ATTN: CC-OPS-WR, H. Wilson
ATTN: CC-OPS-W

US Army Comm R&D Command
ATTN: DRDCO-COM-RY, W. Kesselman

US Army Foreign Science & Tech Ctr
ATTN: DRXST-SD

US Army Materiel Dev & Readiness Cmd
ATTN: DRCLDC, J. Bender

US Army Nuclear & Chemical Agency
ATTN: Library

US Army Satellite Comm Agency
ATTN: Document Control

DEPARTMENT OF THE ARMY (Continued)

US Army TRADOC Sys Analysis Actvy
ATTN: ATAA-TDC
ATTN: ATAA-PL
ATTN: ATAA-TCC, F. Payan Jr

USA Missile Command
ATTN: DRSMI-YSO, J. Gamble

DEPARTMENT OF THE NAVY

Joint Cruise Missiles Project Ofc
ATTN: JCMG-707

Naval Air Systems Command
ATTN: PMA 271

Naval Elec Sys Command
ATTN: PME 106-13, T. Griffin
ATTN: PME 117-2013, G. Burnhart
ATTN: PME 117-211, B. Kruger
ATTN: Code 501A
ATTN: Code 3101, T. Hughes
ATTN: PME 106-4, S. Kearney
ATTN: PME 117-20

Naval Intelligence Support Ctr
ATTN: NISC-50

Naval Ocean Sys Center
ATTN: Code 5322, M. Paulson
ATTN: Code 5323, J. Ferguson
ATTN: Code 532

Naval Research Lab
ATTN: Code 7500, B. Wald
ATTN: Code 4780, S. Ossakow
ATTN: Code 4720, J. Davis
ATTN: Code 4780
ATTN: Code 4700
ATTN: Code 6700
ATTN: Code 4187
ATTN: Code 7950, J. Goodman

Naval Space Surveillance Sys
ATTN: J. Burton

Naval Surface Weapons Center
ATTN: Code F31

Naval Telecommunications Command
ATTN: Code 341

Ofc of the Deputy Chief of Naval Ops
ATTN: OP 981N
ATTN: OP 941D
ATTN: NOP 65, Strat Thtr Nuc Warf Div

Office of Naval Research
ATTN: Code 412, W. Condell
ATTN: Code 414, G. Joiner

Strat Sys Project Office
ATTN: NSP-2722, F. Wimberly
ATTN: NSP-2141
ATTN: NSP-43

DEPARTMENT OF THE AIR FORCE

Aerospace Defense Command
ATTN: DC, T. Long

DEPARTMENT OF THE AIR FORCE (Continued)

Air Force Geophysics Lab
ATTN: OPR, H. Gardiner
ATTN: OPR-1
ATTN: LKB, K. Champion
ATTN: CA, A. Stair
ATTN: R. O'Neil
ATTN: PHP
ATTN: PHI, J. Buchau
ATTN: R. Babcock

Air Force Tech Applications Ctr
ATTN: TN

Air Force Weapons Lab, AFSC
ATTN: NTYC
ATTN: SUL
ATTN: NTN

Air Force Wright Aeronautical Lab
ATTN: W. Hunt
ATTN: A. Johnson

Air Logistics Command
ATTN: OO-ALC/MM

Air University Library
ATTN: AUL-LSE

Air Weather Service, MAC
ATTN: DNXP, R. Prochaska

Assistant Chief of Staff
Studies & Analyses
ATTN: AF/SASC, W. Kraus
ATTN: AF/SASC, C. Rightmeyer

Ballistic Missile Office
ATTN: ENSN, W. Wilson
ATTN: SYC, Col Kwan

Deputy Chief of Staff
Research, Development, & Acq
ATTN: AFRDSS
ATTN: AFRDSP
ATTN: AFRDS, Space Sys & C3 Dir

Deputy Chief of Staff
Operations & Plans
ATTN: AFXOKT
ATTN: AFXOKS
ATTN: AFXOKCD

Deputy Chief of Staff
Operations & Plans
ATTN: AFXOXFD

Electronic Systems Div,
ATTN: SCT-2, J. Clark

Electornic Systems Div
ATTN: ESD/SCT-2, Lt Col J. Clark

Elec Sys Div
ATTN: OCT-4, J. Deas
ATTN: YSM, J. Kobelski
ATTN: YSEA

Foreign Tech Div, AFSC
ATTN: TQTD, B. Ballard
ATTN: NIIS Library

DEPARTMENT OF THE AIR FORCE (Continued)

Rome Air Development Center, AFSC
ATTN: OCS, V. Coyne
ATTN: TSLD

Rome Air Development Center, AFSC
ATTN: EEP, J. Rasmussen

Space Division
ATTN: YGJB, W. Mercer
ATTN: YKM, Maj Alexander
ATTN: YKM, Capt Norton

Strategic Air Command
ATTN: XPFS
ATTN: DCX
ATTN: ADWATE, B. Bauer
ATTN: NRT
ATTN: DCXT, T. Jorgensen

FOREIGN AGENCY

Nato School, SHAPE
ATTN: US Document Officer

OTHER GOVERNMENT AGENCIES

Central Intelligency Agency
ATTN: OSWR/NED
ATTN: OSWR/SSD for K. Feuerpfetl

Department of Commerce
National Bureau of Standards
ATTN: Sec Ofc for R. Moore

Department of Commerce
National Oceanic & Atmospheric Admin
ATTN: R. Grubb

Institute for Telecommunication Sciences
ATTN: A. Jean
ATTN: W. Utlaut
ATTN: L. Berry

DEPARTMENT OF ENERGY CONTRACTORS

EG&G, Inc
ATTN: J. Colvin
ATTN: D. Wright

University of California
Lawrence Livermore National Lab
ATTN: L-31, R. Hager
ATTN: L-389, R. Ott
ATTN: Technical Info Dept Library

Los Alamos National Laboratory
ATTN: P. Keaton
ATTN: C. Westervelt
ATTN: R. Jeffries
ATTN: T. Kunkle, ESS-5
ATTN: D. Simons
ATTN: MS 664, J. Zinn
ATTN: MS 670, J. Hopkins
ATTN: J. Wolcott

Sandia National Labs, Livermore
ATTN: T. Cook
ATTN: B. Murphey

DEPARTMENT OF ENERGY CONTRACTORS (Continued)

Sandia National Lab
ATTN: D. Dahlgren
ATTN: D. Thornbrough
ATTN: 3141
ATTN: Org 4231, T. Wright
ATTN: Space Project Div
ATTN: Org 1250, W. Brown

DEPARTMENT OF DEFENSE CONTRACTORS

Berkeley Research Associates, Inc
ATTN: J. Workman
ATTN: S. Brecht
ATTN: C. Prettie

Boeing Aerospace
ATTN: MS/87-63, D. Clauson

Boeing Co
ATTN: S. Tashird
ATTN: G. Hall

Booz-Allen & Hamilton, Inc
ATTN: B. Wilkinson

BR Communications
ATTN: J. McLaughlin

University of California at San Diego
ATTN: H. Booker

Charles Stark Draper Lab, Inc
ATTN: D. Cox
ATTN: J. Gilmore
ATTN: A. Tetewski

Computer Sciences Corp
ATTN: F. Eisenbarth

Comsat Labs
ATTN: G. Hyde
ATTN: D. Fang

Cornell University
ATTN: M. Kelly
ATTN: D. Farley Jr

E-Systems, Inc
ATTN: R. Berezdivin

Electrospace Systems, Inc
ATTN: H. Logston
ATTN: P. Phillips

ESL, Inc
ATTN: E. Tsui
ATTN: R. Ibaraki
ATTN: R. Heckman
ATTN: J. Marshall
ATTN: J. Lehman

General Electric Co
ATTN: C. Zierdt
ATTN: A. Steinmayer

General Research Corp
ATTN: B. Bennett

DEPARTMENT OF DEFENSE CONTRACTORS (Continued)

General Electric Co
ATTN: G. Millman
ATTN: F. Reibert

Geo-Centers, Inc
ATTN: E. Marram

Harris Corp
ATTN: E. Knick

Horizons Technology, Inc
ATTN: R. Kruger

HSS, Inc
ATTN: D. Hansen

IBM Corp
ATTN: H. Ulander

Institute for Defense Analyses
ATTN: H. Gates
ATTN: E. Bauer
ATTN: H. Wolfhard
ATTN: J. Aein

International Tel & Telegraph Corp
ATTN: Tech Library

International Tel & Telegraph Corp
ATTN: G. Wetmore

JAYCOR
ATTN: J. Sperling

JAYCOR
ATTN: J. Doncarlos

Johns Hopkins University
ATTN: J. Phillips
ATTN: T. Evans
ATTN: J. Newland
ATTN: P. Komiske

Kaman Sciences Corp
ATTN: T. Stephens

Kaman Tempo
ATTN: DASIAC
ATTN: W. Knapp
ATTN: W. McNamara
ATTN: K. Schwartz
ATTN: J. Devore

Litton Systems, Inc
ATTN: B. Zimmer

Lockheed Missiles & Space Co, Inc
ATTN: R. Sears
ATTN: J. Kumer

Lockheed Missiles & Space Co, Inc
ATTN: C. Old
ATTN: D. Churchill
ATTN: Dep 60-12

MIT Lincoln Lab
ATTN: D. Towle

DEPARTMENT OF DEFENSE CONTRACTORS (Continued)

MA/COM Linkabit Inc
ATTN: A. Viterbi
ATTN: I. Jacobs
ATTN: H. Van Trees

Magnavox Govt & Indus Elec Co
ATTN: G. White

Martin Marietta Corp
ATTN: R. Heffner

McDonnell Douglas Corp
ATTN: Technical Library Services
ATTN: R. Halprin
ATTN: H. Spitzer
ATTN: W. Olson

Mission Research Corp
ATTN: R. Bogusch
ATTN: R. Bigoni
ATTN: C. Lauer
ATTN: F. Fajen
ATTN: R. Kilb
ATTN: S. Gutsche
ATTN: R. Hendrick
ATTN: G. McCartor
ATTN: Tech Library
ATTN: F. Guigliano

Mitre Corp
ATTN: A. Kymmel
ATTN: C. Callahan
ATTN: MS J104, M. Dresp
ATTN: G. Harding
ATTN: B. Adams

Mitre Corp
ATTN: M. Horrocks
ATTN: W. Hall
ATTN: J. Wheeler
ATTN: W. Foster

Pacific-Sierra Research Corp
ATTN: F. Thomas
ATTN: H. Brode, Chairman SAGE
4 cy ATTN: E. Field Jr

Pennsylvania State University
ATTN: Ionospheric Research Lab

Photometrics, Inc
ATTN: I. Kofsky

Physical Dynamics, Inc
ATTN: E. Fremouw

Physical Research, Inc
ATTN: R. Deliberis

R&D Associates
ATTN: B. Yoon

Science Applications, Inc
ATTN: L. Linson
ATTN: E. Straker
ATTN: D. Hamlin
ATTN: C. Smith

DEPARTMENT OF DEFENSE CONTRACTORS (Continued)

R&D Associates
ATTN: W. Karzas
ATTN: W. Wright
ATTN: C. Greifinger
ATTN: R. Lelevier
ATTN: F. Gilmore
ATTN: B. Gabbard
ATTN: H. Ory
ATTN: R. Turco
ATTN: M. Gantsweg

Rand Corp
ATTN: E. Bedrozian
ATTN: C. Crain

Riverside Research Institute
ATTN: V. Trapani

Rockwell International Corp
ATTN: R. Buckner

Rockwell International Corp
ATTN: S. Quilici

Santa Fe Corp
ATTN: D. Paolucci

Science Applications, Inc
ATTN: SZ

Science Applications, Inc
ATTN: J. Cockayne

Stewart Radiance Laboratory
ATTN: J. Ulwich

Sylvania Systems Group
ATTN: R. Steinhoff

Technology International Corp
ATTN: W. Boquist

Analytical Systems Engineering Corp
ATTN: Radio Sciences

Analytical Systems Engineering Corp
ATTN: Security

BDM Corp
ATTN: L. Jacobs
ATTN: T. Neighbors

DEPARTMENT OF DEFENSE CONTRACTORS (Continued)

SRI International
ATTN: G. Price
ATTN: R. Tsunoda
ATTN: J. Vickrey
ATTN: W. Chesnut
ATTN: D. Neilson
ATTN: J. Petrickes
ATTN: R. Leadabrand
ATTN: D. McDaniels
ATTN: R. Livingston
ATTN: M. Baron
ATTN: A. Burns
ATTN: C. Rino
ATTN: W. Jaye
ATTN: G. Smith
ATTN: V. Gonzales

Strategic Systems Div
ATTN: J. Concordia
ATTN: I. Kohlberg

TRI-COM, Inc
ATTN: D. Murry

TRW Electronics & Defense Sector
ATTN: D. Dee
ATTN: R. Plebuch

Utah State University
ATTN: Sec Con Ofc for D. Burt
ATTN: Sec Con Ofc for K. Baker, Dir Atmos & Space Sci
ATTN: Sec Con Ofc for L. Jensen
ATTN: Sec Con Ofc for A. Steed

Visidyne, Inc
ATTN: J. Carpenter
ATTN: C. Humphrey
ATTN: W. Reidy
ATTN: O. Sheppard

Aerospace Corp
ATTN: I. Garfunkel
ATTN: D. Olsen
ATTN: J. Straus
ATTN: V. Josephson
ATTN: T. Salmi
ATTN: R. Slaughter

Meteor Communications Corp
ATTN: R. Leander


DA
FILM